ANISOTROPIC STRUCTURE TO CONTROL NUCLEATION AND PROPAGATION: FRACTURE DIODES

The contents of this chapter are also presented in "Fracture Diodes: Directional Asymmetry of Fracture Toughness" by N.R. Brodnik, S. Brach, C.M. Long, K. Bhattacharya, B. Bourdin, K.T. Faber, and G. Ravichandran, which is currently in preparation. N.R. Brodnik led the experimental portion of the work, and was assisted by C.M. Long. S. Brach led the numerical simulations. Bhattacharya and Bourdin supervised the numerical simulations while Faber and Ravichandran supervised the experimental work. All authors were involved in discussing all aspects of the work, and preparing the manuscript.

0.1 Introduction

In the previous chapter, the effect of anisotropic structure on fracture properties was discussed in the context of the effect of inclusion structure on crack propagation. Surfing load experiments were used to provide stable crack growth, but all observations of mechanical response were made well within the crack propagation regime, and crack tip position was always readily identifiable. However, if designed anisotropy is to be suitable as a toughening mechanism in practical applications, the anisotropic structures must be able to function in scenarios where loading occurs well before macro-scale crack propagation has begun. This means exploring the effects of designed anisotropic structure on both nucleation and propagation of the crack.

The surfing load experiments explored in Chapter 2 provided a promising means to investigating designed anisotropy under stable crack growth conditions, but some characterization limitations arose when exploring anisotropic structures. The first limitation was related to crack pinning and subsequent unstable propagation events. Because load progression was displacement controlled, stability was lost during nucleation and renucleation events because the crack would arrest, but the sample would continue to be loaded as it travelled along the diverging rail. This load buildup led to sudden propagation events, where the crack would propagate too quickly to be properly characterized. The second limitation with the surfing load condition was related to directionality. Because the surfing load applies a controlled load from a single direction, anisotropic toughness can only be explored by directly characterizing and comparing the toughness values of anisotropic structures from different orientations, which can prove difficult due to the already mentioned crack

pinning and unstable propagation.

The focus of this chapter is to demonstrate the influence of designed directional asymmetry on bulk fracture under loading scenarios that do not require stable growth of a preexisting crack. These scenarios were investigated by changing the loading condition to be unbiased, and exploring failure from a phenomenological standpoint. Under unbiased loads, such as uniaxial tension, because failure is equally possible from multiple directions, the effect of structural asymmetry manifests through consistent fracture from a particular direction rather than as differences in fracture toughness. The possibility of this was suggested in numerical simulations by Hossain et al.[1] through the exploitation of material architecture that lacks mirror symmetry. Consistent directional failure under unbiased loading also inspired the name "fracture diodes" for specimens exhibiting this phenomenon. The current work explores the potential of this phenomenon through numerical simulation, and demonstrates it experimentally by realizing asymmetric microstructures through 3D printing of a brittle photopolymer.

0.2 Methods

0.3 Specimen Design

Since this investigation was centered on the mode and direction of the failure event rather than the measured toughness, the design for the fracture diode specimens was chosen to be relatively simple. The asymmetric inclusions were chosen to be triangles and the inclusion phase was chosen to be a void, rather than the partial changes in thickness used in the surfing load investigations. This meant that in addition to the voids acting as a compliant inclusion phase, any cracks that formed in the brittle polymer would have to renucleate out of each void, allowing for investigations into both nucleation and propagation. This simple arrangement of triangular voids was also well-suited to numerical investigation, as continuum simulations of a single phase with voids are not less computationally demanding than more complex structures. An example of a simulation domain and analogous printed specimen is shown in Figure 0.1.

0.3.1 Numerical Methods

Variational phase-field simulations Similar to the surfing load tests, crack propagation in the fracture diodes was investigated numerically through the variational fracture approach developed by Bourdin et al.[2, 3] For these numerical analyses, the photopolymer system was treated as a perfectly-brittle elastic material. The crack

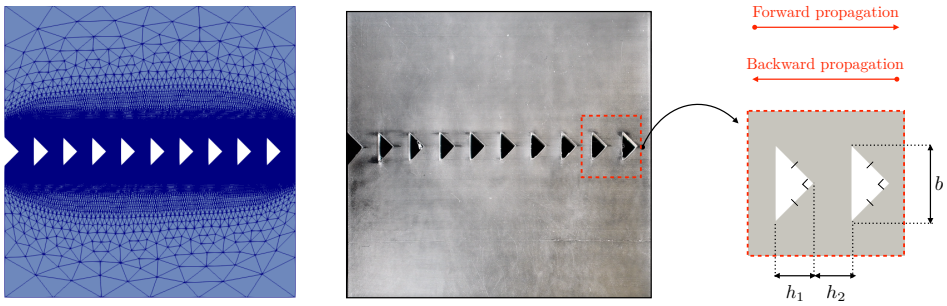

Figure 0.1: An example pattern of asymmetric triangular voids used for the numerical simulations (left) and experimental tests (middle). The inset (right) shows the relevant geometrical parameters of the triangular voids as well as the directions of crack propagation considered in this study, labeled here as 'forward' and 'backward' with respect to void orientation.

propagates through this established domain as a damage phase rather than a strict discontinuity, with completely damaged phase being unable to bear any load. Within this domain, the brittle phase through which the crack travels is discretized into a mesh structure and the crack has an established nucleation length which describes both its half-width and the minimum discrete length over which it can nucleate or propagate. The mesh structure used to describe the homogeneous brittle phase is chosen to be much smaller than the characteristic nucleation length in the area around the inclusions, but is then coarsened away from the inclusions for computational efficiency. An example mesh is shown in Figure 0.1.

The fracture problem is solved by alternatively minimizing the total energy functional with respect the two state variables, which are the damage phase and the displacement. The constrained minimization with respect to the damage phase is implemented using the variational inequality solvers provided by `PETSc` [4–6], whereas the minimization with respect to displacement field is a linear problem, solved by using preconditioned conjugated gradients. All computations are performed by means of the open source code `mef90`[1].

All equations used in the numerical analyses are non-dimensionalized, and geometrical parameters are chosen to match the experimental configurations chosen for the printed diode structures.

Numerical Load Configurations The focus of this investigation was to look at the phenomenological aspects of failure and evaluate how designed anisotropy could

[1] Available at `https://www.bitbucket.org/bourdin/mef90-sieve`.

influence failure mode under unbiased load. In this study, the unbiased load was chosen to be uniaxial tension because it is relatively simple to apply both numerically as well as experimentally. However, tensile load produces unstable crack growth, which can prove difficult to evaluate in extremely brittle materials. In the case of the ideally brittle and purely elastic material system used in numerical simulations, the unstable aspect of tension proved to be a significant challenge because the entire brittle system would fail within a single time step, making observation of the directionality of failure infeasible. Attempts were made to introduce both numerical and material viscosity into the system to slow the crack, but these proved ineffective.

Despite this difficulty, the numerical simulations still have the benefit of much easier design adjustment and mechanical evaluation over the actual experiment. Therefore, it proved sensible to adjust the load configuration in the numerical analysis to allow for slower, more stable crack propagation and use a more formal evaluation technique to justify the expected failure phenomena in the uniaxial tension experiments. For this reason, all numerical experiments were done under the surfing load conditions used in Chapter 2, and the macroscopic effective toughnesses of different orientations were evaluated using the J-integral. These J-integral values were used as a basis for assessing which failure modes were favorable and unfavorable within the diode specimens.

Evaluation of effective toughness As previously discussed, there does not formally exist any theoretical homogenization model able to predict the effective toughness of heterogeneous media. However, using a conceptual extension of classical fracture mechanics theories [7–9], it is reasonable to define the macroscopic resistance to fracture as the maximum value of the far-field energy-release rate as the crack propagates throughout the material. [1, 10]

At each time step, the driving force necessary to sustain the macroscopic crack propagation is determined by computing the energy-release rate using the J-integral at the domain boundary.[7, 9] Therefore, the effective fracture toughness is defined as the energy needed to propagate the crack over a macroscopic distance. This corresponds to the peak value of the energy-release rate, that is, the maximum value of the J-integral over time. This is analogous to the far field J-Integral approach used in Chapter 2, although for this investigation, it is only done in the numerical assessment to provide a formal basis for what failure modes should be favorable or unfavorable under the unbiased load of uniaxial tension. Using this combination of

surfing load for stable crack growth and macroscopic far-field J-integral, a suitable basis can be established for what types of failure are energetically favorable and would therefore be expected in uniaxial tension experiments.

0.3.2 Experimental Methods

Sample Fabrication For the experimental tests, samples were printed using digital light processing (DLP) printing on an Autodesk Ember 3D Printer (Autodesk, San Rafael, CA). Samples were made from commercially available Standard Clear PR48 printing resin, a urethane acrylate photopolymer. To keep comparisons of void arrangements as consistent as possible, all voids were kept to a standard size and structure, namely isosceles right triangles with a vertical hypotenuse which has a fixed length of 3 mm, as shown in Figure 0.2. Similar to the anisotropic inclusions discussed in Chapter 2, the effect of anisotropy should be visible in inclusions of any size scale, so the only factor limiting the size of the triangular voids is the resolution at which anisotropic geometries can be produced. For this study, the triangle size was chosen to make both sample fabrication and failure observation straightforward. This size scale is also well suited to the overall size of the specimen, as each void has a vertical length of 3mm and a horizontal width of 1.5 mm, which scale nicely as clean fractions of the specimen gauge length and width. All specimens tested had a gauge length of 60 mm, with gauge width changing slightly between 28.5 and 31.5 mm depending on design, to preserve symmetry.

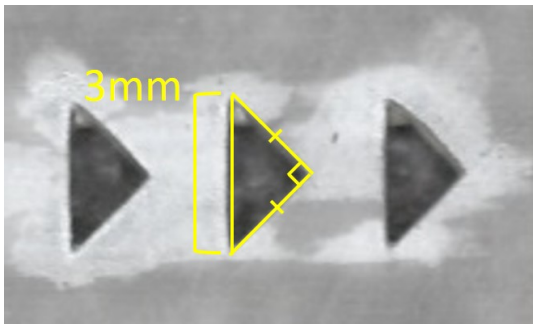

Figure 0.2: Close-up dimensioned view of void pattern used in the printed diode structures, showing the exact size of the isosceles triangle voids.

Using this 3 mm tall, 1.5 mm wide isosceles triangle void design as a standard, a variety of heterogeneous structures were developed to investigate the effect on failure behavior of different structural arrangement parameters, such as void spacing, angle and direction. First, to investigate the influence of spacing, samples with a single row of unidirectional triangular voids were printed with the voids at different

incremental spacing. To look at the effects of void direction on failure behavior, additional designs were printed with bidirectional arrangements of voids that pointed outward from the center of the specimen. To investigate the effects of nucleation and the role of the edge notch, unidirectional specimens were printed both with and without symmetric edge notches. Unidirectional and bidirectional samples shown in Figure 0.3 had a gauge width of 30 mm, while specimens with no edge notch shown in Figure 0.4(a-c) had a gauge width of 28.5 mm and specimens with two edge notches shown in Figure 0.4(d-f) had a gauge width of 31.5 mm. Finally, using the knowledge provided from the failure distributions of these designs, a final design was printed with a custom inclusion morphology and spacing distribution, which was designed to maximize anisotropic fracture behavior.

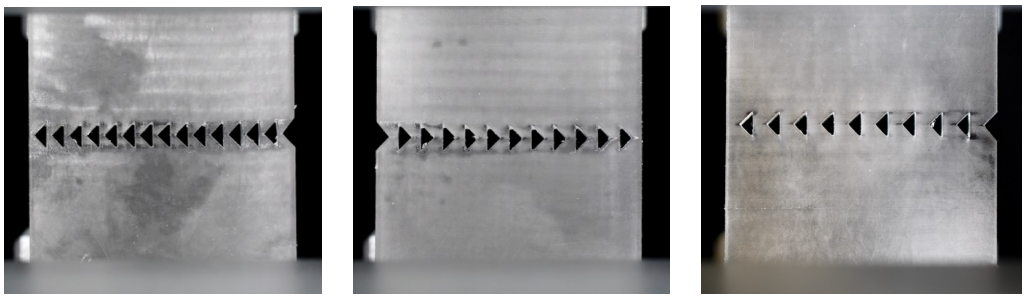

(a) Unidirectional: 0.5 mm Spacing

(b) Unidirectional: 1.0 mm Spacing

(c) Unidirectional: 1.5 mm Spacing

(d) Bidirectional: 0.5 mm Spacing

(e) Bidirectional: 1.0 mm Spacing

(f) Bidirectional: 1.5 mm Spacing

Figure 0.3: Images showing the unidirectional single-notch (a-c) and bidirectional (d-f) designs investigated to understand orientation dependence. Gauge width for all specimens shown is 30 mm.

Accounting for Material Variability Across each of the aforementioned configurations, much consideration had to be given to what aspects of mechanical response could be suitably measured and compared across different configurations. Because samples are composed of a brittle photopolymer, it is critical to distinguish mechanical variations due to material response from variations due to difference in

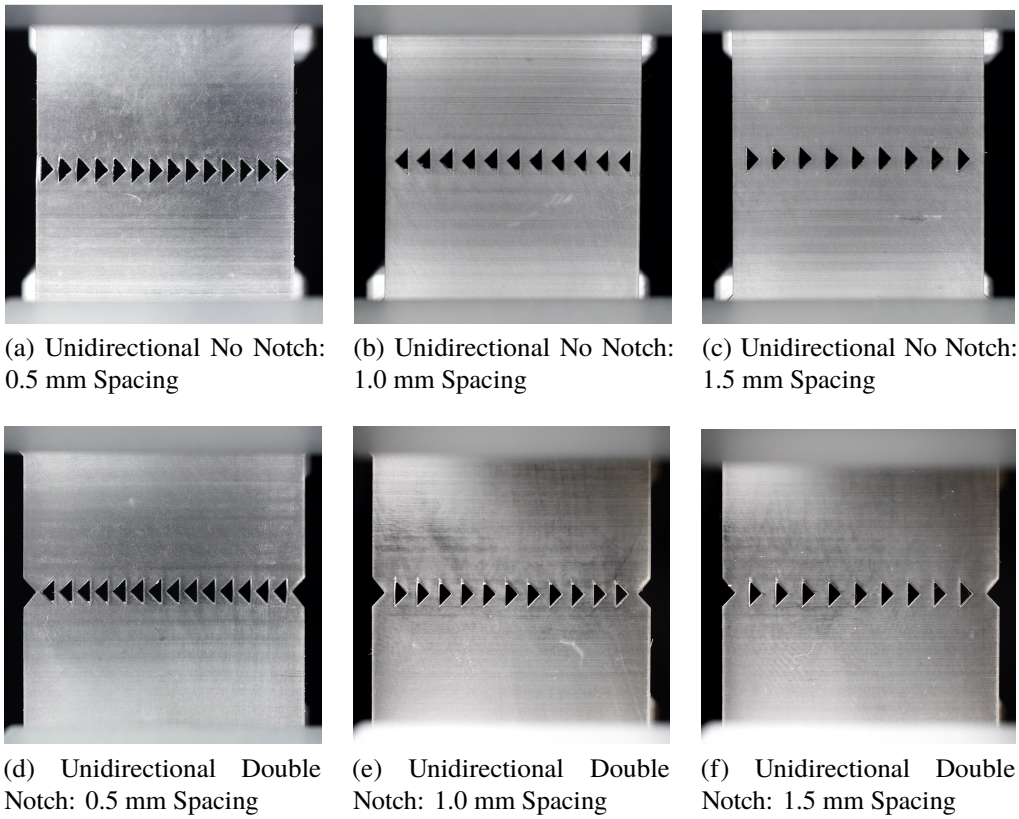

(a) Unidirectional No Notch: 0.5 mm Spacing

(b) Unidirectional No Notch: 1.0 mm Spacing

(c) Unidirectional No Notch: 1.5 mm Spacing

(d) Unidirectional Double Notch: 0.5 mm Spacing

(e) Unidirectional Double Notch: 1.0 mm Spacing

(f) Unidirectional Double Notch: 1.5 mm Spacing

Figure 0.4: Images showing unidirectional no notch (a-c) and unidirectional double notch (d-f) designs investigated to understand edge notch dependence. The gauge width for specimens (a-c) is 28.5 mm and the gauge with for specimens (d-f) is 31.5 mm to preserve symmetry.

the structure or positioning of voids. To minimize the influence of the material on mechanical response, samples were printed using relatively uniform print exposure times (2.2-3.0 seconds per exposure) and were not treated with a UV post-cure. This helped ensure that all samples tested had relatively comparable amounts of UV cross-linking at time of testing. Additionally, all samples were tested within one hour after printing to minimize any embrittlement or bleaching from photo-oxidation.

Mechanical Testing Testing was done on an Instron 5892 (Instron, Norwood, MA) load frame at a constant displacement rate of 1 mm/min and different replicates of each sample type were rotated and mirrored in different ways to ensure that no bias was introduced due to the innate directionality of the DLP printing process. For each arrangement of inclusions, a minimum of 30 replicates were tested. Within these arrangements, a minimum of 8 replicates were tested for each spacing, with the exception of double notch samples with 1 mm spacing, which only had 4 replicates

due to printing errors.

For each test, the load and displacement were recorded using from the load cell and the failure behavior of the sample itself was recorded with a Nikon D7500 (Nikon, Tokyo, Japan) digital camera at a rate of 30 frames per second. Recording was started just before the beginning of load application so that loading data and video could be synchronized through visible failure events.

After testing, video recordings of failure were then reviewed frame-by-frame using the post production film software DaVinci Resolve (Blackmagic Design, Port Melbourne, Australia) to classify their failure behavior and compare with the failure modes predicted by numerical simulation.

0.4 Mechanics of Diode Failure

0.4.1 Numerical Computations

Numerical investigation of directionality is done using the surfing load condition, which limits instantaneous crack growth and unstable snap-throughs. This setting promotes the quasi-static interaction between the crack set and the holes, thus highlighting the occurrence of directionality effects.

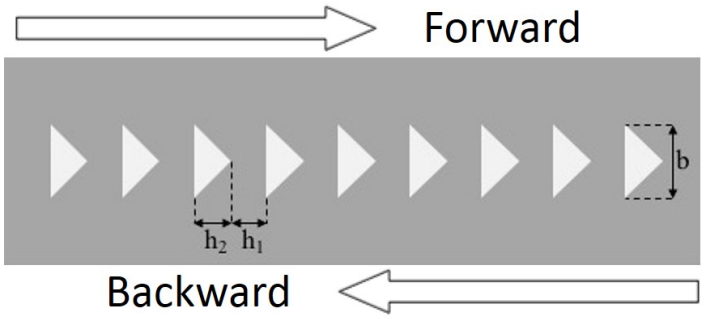

Figure 0.5: Schematic void pattern showing triangle dimensions as well as forward and backward propagation directions.

Consider a specimen with a row of triangular holes as shown in Figure 0.5. The geometry of the voids is expressed in terms of the triangle height, b, triangle spacing, h_1, and triangle width, h_2. First, the specimen is loaded with a surfing boundary condition to macroscopically drive crack propagation in the 'forward' direction, that is from the left to the right side of the specimen. The results in Figure 0.6 show that the crack nucleates at the left notch and rapidly propagates afterwards until it reaches the first triangular hole. The crack then gets pinned at the triangular hole until it

renucleates at the tip and continues to propagate in a left-to-right sense. It should be noted that, although significant damage buildup is observed at the triangle tip, when fracture does occur, each ligament instantaneously fractures without any preferred orientation at the local length-scale. Overall, though, the crack is observed to macroscopically propagate in the forward direction, following the applied boundary condition.

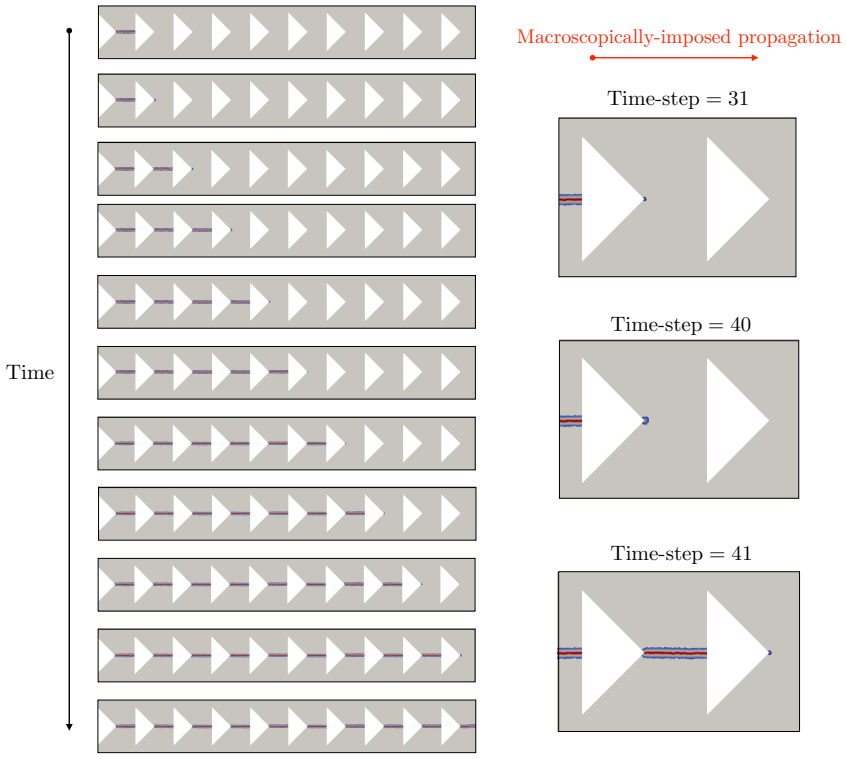

Figure 0.6: Numerical computations showing crack propagation in the forward, or favorable, direction. Left: crack path computed at different timesteps. Right: close-up view of the snapshots of the simulation showing the damage field when a crack is pinned at the hole; note that the damage always initiates at the tip of the triangular hole.

The second numerical experiment is performed by flipping the specimen with respect to the direction imposed for crack propagation by virtue of the placement of the edge notch, as shown in Figure 0.7. In other words, the biased load is now macroscopically driving the crack in the 'backward' direction, that is from the right side to the left side of the original configuration. Note that even though the triangular holes within the domain are mirrored, the edge notch is preserved to allow for identical nucleation behavior between configurations and ensure that the 'forward' and 'backward' analysis are directly comparable. Results in Figure 0.7 show that the crack rapidly

grows through the specimen, by getting pinned and subsequently renucleating at each triangle. Similar to the 'forward' case, failure within each solid segment between voids is unstable and instantaneous, but when the crack becomes pinned at a hole, damage buildup can be seen at the tip of the triangle at the next hole. This effect is clearly visible on the rightmost triangle at time step 75 in Figure 0.7. This suggests that in the case of 'backward' propagation, the crack may be locally propagating from right to left, despite macroscopic failure occurring from left to right.

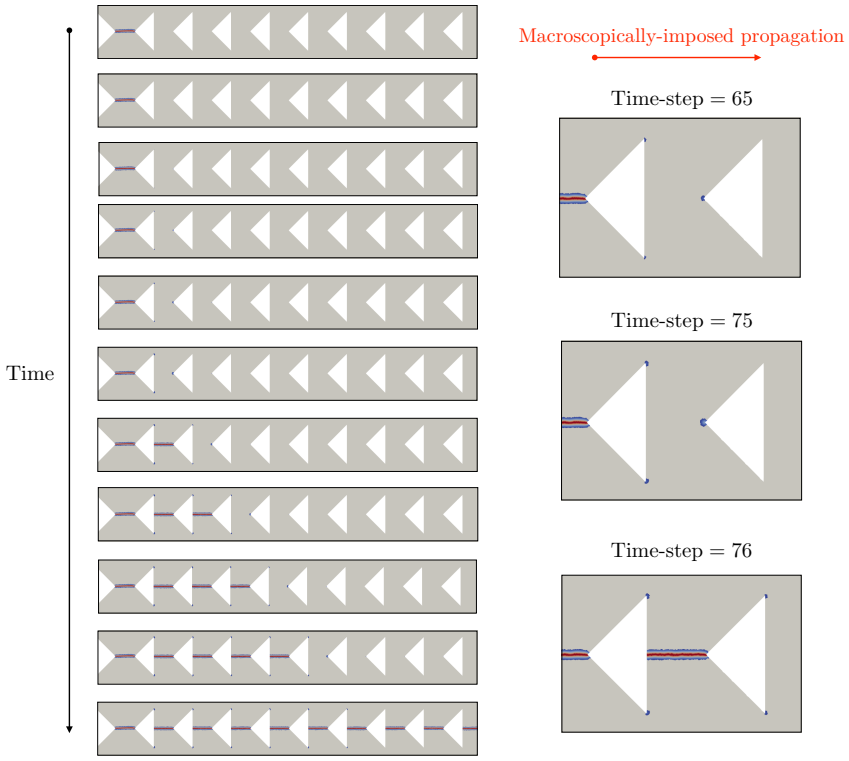

Figure 0.7: Numerical computations showing crack propagation in the backward, or unfavorable, direction. Left: crack path computed at different timesteps. Right: close-up view of the snapshots of the simulation showing the damage field when a crack is pinned at the hole; note that the damage initiates at the tip of the next consecutive triangular hole beyond the pinning site.

In both of these analyses, the driving force necessary to sustain the macroscopic crack propagation is determined by computing the energy-release rate, or J-integral, at the boundary of the specimen.[7, 9] Figure 0.8 shows the evolution of the J-integral as the crack progresses either in the forward or in the backward direction. The J-integral oscillates as the crack interacts with consecutive heterogeneities, with peak values occurring just before unstable propagation through each solid segment. This oscillation also validates the argument that macroscopic toughness of a composite

is based on the peak value of the energy release rate, as this peak value must be reached in order for the crack to propagate over macroscopic distances. As such, the maximum value of the J-integral over the duration of propagation determines the effective fracture toughness of each configuration, and these values are reported in Table 0.1. It should also be noted that, apart from small transient effects well below peak toughness near time t = 0, results are independent of the presence of the initial notch.

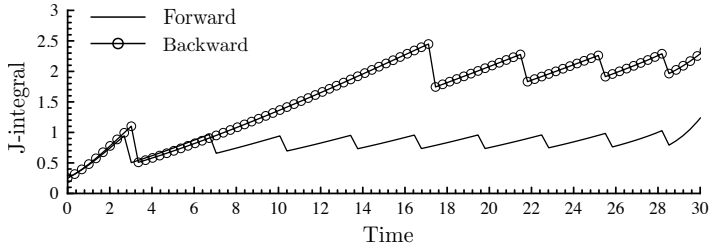

(a)

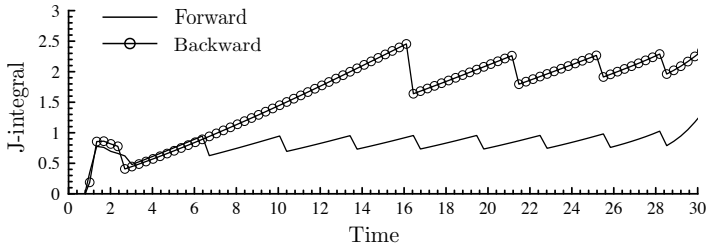

(b)

Figure 0.8: Numerical computations. Evolution of the J-integral with time as the crack is propagated through the specimens shown in Figures 0.6 (a) and 0.7 (b) with $h_1 = h_2$.

Table 0.1: Numerical computations. The computed effective toughness, that is, the maximum toughness value measured in the J-integral over the entire time duration, is shown in Figure 0.1 for both the forward and backward directions for various spacings h_2. The results are normalized with respect to the toughness of the uniform material, which is set to be J = 1.

	$h_2 = 4h_1$	$h_2 = 2h_1$	$h_2 = h_1$	$h_2 = h_1/2$	$h_2 = h_1/4$
Forward	1.4418	1.2550	0.9630	0.6712	0.4556
Backward	3.2765	3.1065	2.2692	1.1295	0.5906

Following this procedure, effective toughness values determined for specimens with

various spacings h_2 are shown in Table 0.1, expressed as a function of hole width h_1. All numerically determined toughness values are normalized with respect to the toughness of the intact material which has a J-integral value of 1. When $h_1 = h_2$, the effective toughness has a normalized value of 0.963 when propagating forward, which is far lower than the value of 2.27 in the backward direction. This trend of toughness in the forward direction being lower than the backward holds true regardless of spacing, though the difference in magnitude between the two directions varies with different spacings. It is straightforward to conclude that the resistance to crack propagation is asymmetric and depends on the sense of propagation, with the favorable growth direction being the 'forward' direction, and the unfavorable growth direction being the 'backward' direction.

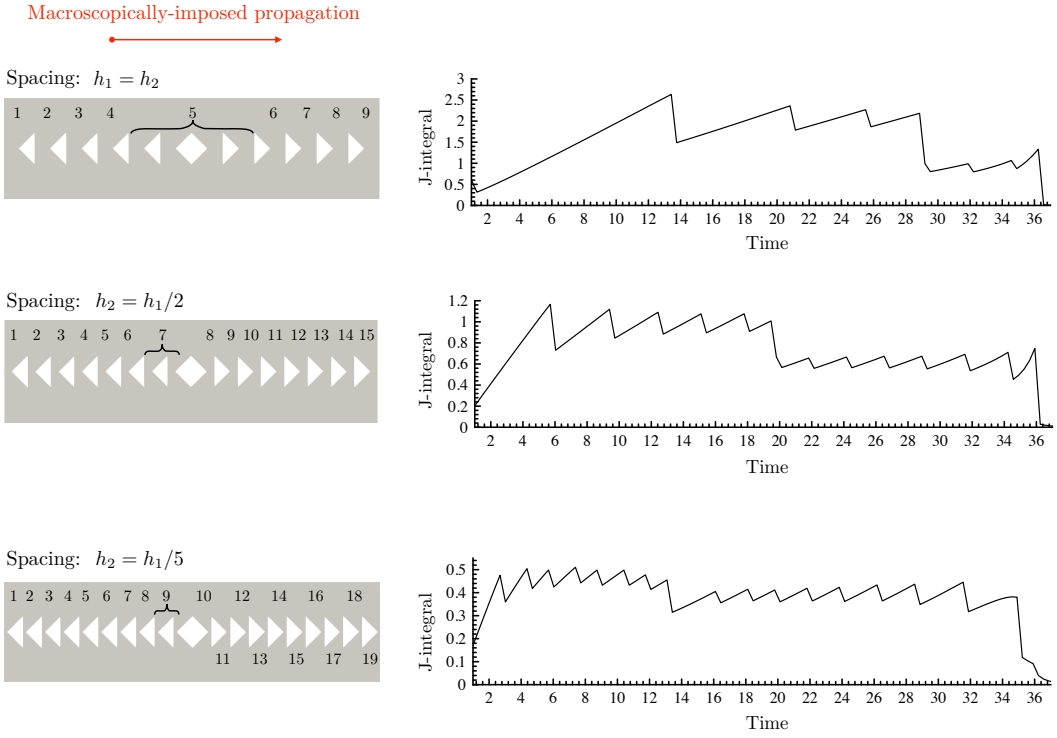

Figure 0.9: Numerical computations for bidirectional fracture diodes: crack paths and J-integrals shown for various values of spacing h_2. Numbers indicate the sequential failure of individual ligaments.

In the numerical analysis of bidirectional arrangements, the directional dependence on void orientation is present in a manner similar to that of the unidirectional arrangements, but some challenges arise due to the bias introduced by the surfing load condition. The computed crack path and J-integral are shown in Figure 0.9 for various values of the spacing h_2 while the size h_1 of the heterogeneity is kept constant.

The surfing condition introduces bias here by forcing the crack to nucleate at the left side of the specimen, resulting in the first half of the specimen exhibiting unfavorable propagation and the second half of the specimen exhibiting favorable propagation. Initially, propagation is unfavorable, as the crack gets pinned at each hole and it has to renucleate at the tip of the next void in order to continue propagating. This behavior continues until the crack approaches the symmetry axis of the specimen, beyond which the voids are oriented in a manner favorable for crack growth. The evolution of the energy-release rate over time clearly shows the sequential rapid propagation events that occur in this fracture process (see Figure 0.9). The transition from unfavorable to favorable orientation of heterogeneities is accompanied by a sudden drop in the macroscopic driving force, which demonstrates clearly the preferential direction of propagation. By extension, it is logical to conclude that under unbiased load, it would be expected for crack growth to occur along the toughness-minimizing path, which would be symmetric propagation outward from the middle of the specimen to each of the two edges.

Regardless of void arrangement, the origin of this asymmetry in effective toughness is fundamentally the lack of mirror symmetry in the void structure. As the crack is driven in the favorable growth direction, it is pinned by each new void, but a new crack can nucleate relatively easily at the tip of the triangular hole, allowing for straightforward propagation. In the unfavorable growth direction, the crack is similarly pinned at each void, but it is difficult for renucleation to occur along the flat edge opposite the triangle tip. This is not surprising, as it is known (e.g., [10, 11]) that cracks have difficulty in renucleating at interfaces where there is a sudden change in elastic modulus. Thus, it requires less energy for the crack to nucleate at the next hole (see Figure 0.7) and to propagate backwards into the current triangular void. As a consequence, the driving force needed to macroscopically drive crack propagation is higher for the unfavorable case.

0.4.2 Experiments

Before different void arrangements can be compared experimentally, it is important to verify that changes in void orientation and arrangement do not dramatically alter the elastic response of the system under uniaxial tension, which would introduce unwanted biases into the failure analysis. To assess this, displacement at the initial failure event in each sample was measured and plotted against the load measured at this first failure event. This relationship is a good indicator of material compliance, and if the compliance is relatively uniform across replicates and designs, the failure

stresses should follow a linear pattern. A plot of failure stress versus time to failure is shown in Figure 0.10.

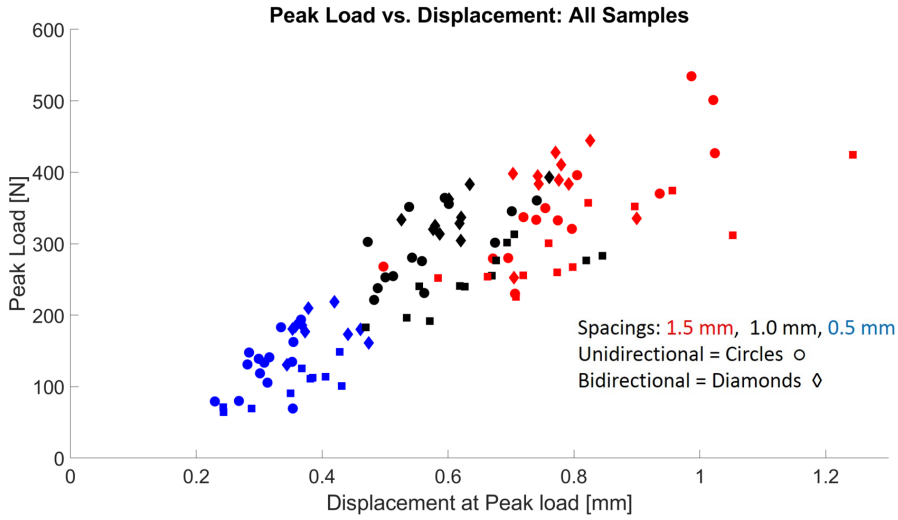

Figure 0.10: Plot of Peak Load versus Displacement for the different void arrangements analyzed in this study.

Although there is some variation, the general pattern of compliance is linear across all specimens. It should be noted that although the peak load reported in Figure 0.10 is not a perfect indicator of the stress state in the sample due to the presence of heterogeneous structure, this was still deemed reasonable under the premise that the specimens would behave like an isostress composite with a thin soft layer (the region containing voids) sandwiched between two thicker stiff layers. Because the stiff layers are much thicker, it was expected that their elastic behavior dominates, so the arrangement of the voids would not have significant effect on compliance. In other words, the elastic behavior of the specimens would be governed by the homogeneous regions, and the failure behavior would be governed by the heterogeneous regions.

During mechanical testing, all specimen failure modes were classified into three mutually exclusive groups. Specimen failure was classified as ‘favorable’ if fracture followed the direction of convergence of the triangular inclusions, consistent with the low toughness pattern predicted by numerical simulations. Analogously, behavior was termed ‘unfavorable’ when the sample failed in the exact opposite of the predicted sequence. Finally, sample failure is ‘random’ if there was no real pattern to failure or if specimen failure occurred too rapidly to be characterized from video recording. Schematic images of ‘expected’ failure behavior in unidirectional and bidirectional void arrangements are shown in Figure 0.11.

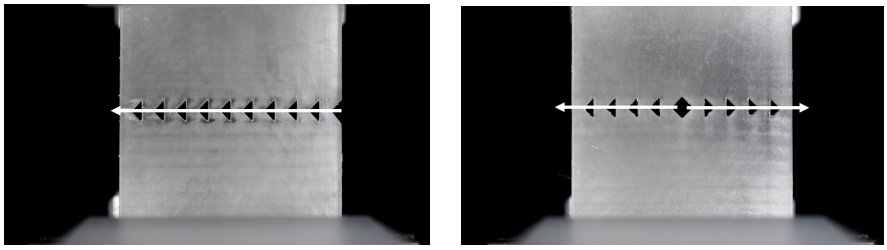

(a) Unidirectional Failure (b) Bidirectional Failure

Figure 0.11: Specimen images with overlayed arrows showing the favorable failure directions for (a) unidirectional, and (b) bidirectional designs.

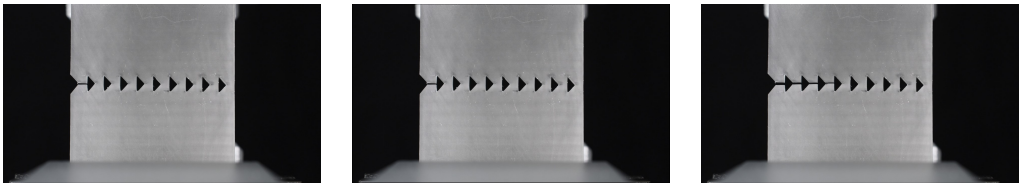

(a) Time = 41 sec, 233 ms (b) Time = 42 sec, 233 ms (c) Time = 43 sec, 233 ms

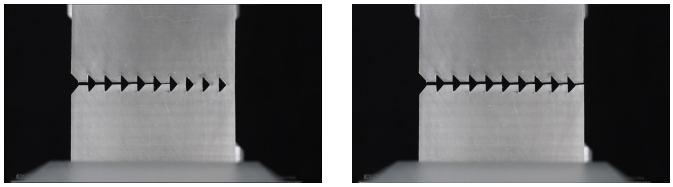

(d) Time = 44 sec, 233 ms (e) Time = 45 sec, 233 ms

Figure 0.12: Time lapse images showing the sequential failure behavior of a unidirectional specimen (mirrored for consistency). A time interval of 1 second passes between each photo in the sequence.

Figure 0.12 shows a series of snapshots of the failure of a representative specimen that was classified as 'favorable'. The crack propagation is locally unstable, with the segments between voids failing rapidly, but the failure of each successive segment is delayed by the voids, which force renucleation into the next segment. Importantly, the crack propagates in the direction of convergence of the triangular voids, nucleating at the tip of each consecutive triangular void before continuing propagation. Additional SEM fractography shown in Figure 0.13 verifies that nucleation of the crack did occur at the tips of the triangular voids, as was predicted by numerical analyses. Furthermore, this directionally dependent behavior was somewhat resilient to the influence of precracking, as the formation of a single segment precrack on the opposite side of the specimen failed to alter the direction of the sequential events in some cases. Though weakest link failure mechanics still dominated the initial failure of segments, the anisotropy of the voids inhibits propagation of the crack in

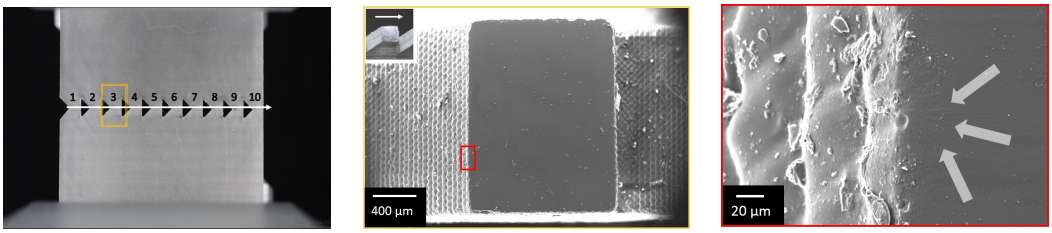

(a) Sample/Segment of Interest (b) Low Magnification SEM (c) High Magnification SEM

Figure 0.13: SEM fractography of a sample that failed in a favorable manner (a) based on simulation predictions, showing that fracture of each diode segment (b) nucleates from the tip of the triangular void inclusions (c). Inset in top left of (b) shows a representative fracture surface to indicate direction of global crack propagation with respect to SEM images.

one direction moreso than the other.

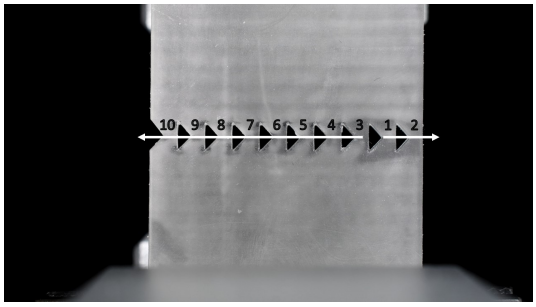

Figure 0.14: Image with a graphical overlay showing the unexpected failure of a unidirectional specimen. The failure events of individual segments are numbered in order from 1 to 10, with 1 being the first failure event and 10 being the last. White arrows indicate the direction of global crack propagation during failure.

Samples that failed in an 'unfavorable' manner also provide additional insight into fracture behavior in systems with directional anisotropy. A particular instance of unfavorable failure is shown in Figure 0.14. The critical defect in the system (as assessed post-fracture) happens to be near the far end of the sample where the crack would normally be expected to terminate. The exact nature of this defect is not clear, as it could be either a print defect or a variation in sharpness in the triangular inclusion at that location. Once the initial failure event occurs near the far right side, the crack propagates in the favorable direction until it reaches the free surface at the end of the sample. At this point, the extended macro-crack is the critical flaw in the system, and it is sufficiently large to drive the remainder of propagation backwards. This clearly demonstrates the trajectory dependence of fracture and how random nucleation events can lead to behavior that would typically be described as unfavorable. Fractographic analysis shown in Figure 0.15 also demonstrates that

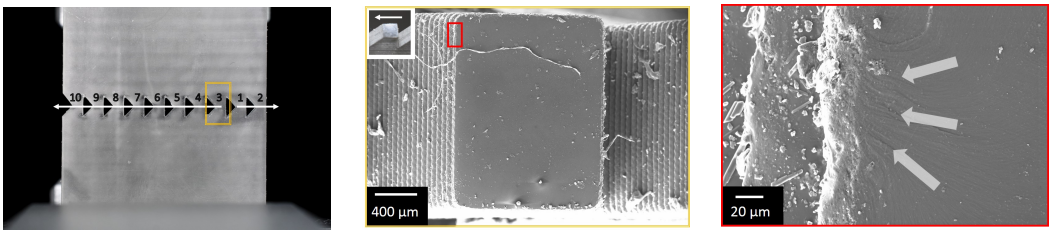

(a) Segment of Interest (b) Low Magnification SEM (c) High Magnification SEM

Figure 0.15: SEM fractography of a sample that failed in in an unexpected manner (a) based on simulation predictions. Even though global crack propagation is in the opposite direction, segment failure (b) still nucleates from the tip of the triangular void inclusions (c), so local failure propagates in the opposite direction of global failure. Inset in top left of (b) shows a representative fracture surface to indicate direction of global crack propagation with respect to SEM images.

even in the case of unfavorable propagation, numerical simulation still accurately predicts the local failure behavior, i.e., when the crack becomes trapped in a given void, it renucleates at the tip of the next consecutive triangular void, making local propagation occur in the opposite direction of macroscopic propagation.

0.5 Statistics of Diode Failure

Once the possible diode failure modes are understood, it makes sense to investigate to what extent the arrangement of asymmetric voids can actually influence failure across many replicates. To that extent, many diode samples were tested across 4 designs and 3 spacings to gain a clearer understanding of how directional asymmetry can influence failure that is otherwise governed by Weibull statistics and weakest link theory.

Table 0.2: Distribution of sample failures for the triangular void arrangements evaluated in this investigation.

Type	Total	Favorable	Random
Unidirectional	42	33	5
Bidirectional	30	19	6
Unidirectional No Notch	34	12	11
Unidirectional Double Notch	50	33	10

The distributions of failure modes for each of the triangular void arrangements tested in this study are shown in Table 0.2. The exact nature of the failure distribution as well as the impact of spacing are discussed in more detail on a case-by-case basis for each arrangement.

0.5.1 Unidirectional Diodes

A total of 42 unidirectional diode samples were tested across 3 different spacings. Of these 42 samples, 33 failed in the favorable mode, with 5 failing randomly and 4 failing unfavorably. This equates to 78% of samples failing in the mode predicted by numerical simulations to be favorable. This 78% favorable failure rate is the first clear indicator that asymmetric void orientation has an influence on the macroscopic failure properties. If the voids had no influence on failure, it would be expected that failure modes were governed solely by natural material flaws, which would follow a Weibull distribution. If this were the case, the number of samples failing favorably would likely be similar to the number of samples failing unfavorably, and the number of random failures would be significantly higher. Although void orientation showed a clear effect on the failure mode in unidirectional structures, no dependence on void spacing was observed.

0.5.2 Bidirectional Diodes

For the bidirectional diode design, a total of 30 samples were tested. Across all three spacings tested, a total of 19 samples failed in the favorable configuration, which in this case was predicted to be failure originating from the symmetrical void at the center of the specimen. Of the remaining 11 samples, 6 failed randomly and 5 failed unfavorably, with unfavorable failure being classified as failure that originated from either edge of the specimen. This equates to failure distribution with a 63% favorable rate, which is again well above the expected value from random flaws and indicates that similar to the unidirectional design, the bidirectional void arrangement has an influence on the mode of failure of the specimen, although in this case it does not produce directional asymmetry, as the arrangement is symmetrical about the center of the specimen. There was also not found to be any significant correlation between void spacing and occurrence of favorable failure, as both random and unfavorable failure events were relatively few in number and reasonably well distributed across all spacings. However, it should be noted that when the unidirectional and bidirectional failure distributions are compared, the unidirectional specimens have a greater tendency to fail favorably by about 15%, which is a noticeable margin given the number of replicates tested for each design. It was suspected that some of this difference may arise from the presence of an edge notch in the unidirectional design. To determine whether or notch this notch was creating a significant difference, additional unidirectional designs were explored.

0.5.3 Edge Notch Effects

To clarify whether or not the disparity in favorable failure rates between unidirectional and bidirectional specimens was due to edge notch effects, additional testing was done on unidirectional designs containing no edge notches as well as unidirectional designs with identical notches on both sides. When the notches were removed from the unidirectional specimens, a dramatic change in the distribution of failure modes was observed. Out of a total of 34 specimens tested across three spacings, only 12 failed in the favorable mode as predicted by numerical analyses. Out of the remaining 22 specimens, 11 failed randomly, and 11 failed unfavorably, leading to a 35% favorable failure rate and creating and almost perfectly uniform distribution of failure between all three modes, which is markedly different than the distribution seen in either the notched unidirectional or bidirectional specimens. This indicates that the presence of an edge notch has an even stronger effect on failure mode than originally expected; when edge notches are removed, failure becomes less dependent on void orientation, and thus failure modes become more random.

To better understand the influence of the edge notch on crack nucleation, an additional unidirectional design was explored with identical edge notches present on both sides of the specimen. For this double-edge notch design, a total of 50 specimens were tested across 3 different spacings. Of these 50 specimens, 33 failed favorably, 10 failed randomly, and 7 failed unfavorably, leading to a 66% favorable failure rate, very similar to that of the bidirectional specimens. Even when present on both sides, the edge notches seem to significantly increase the occurrence of nucleation from the edges of the specimen, which better allows the anisotropy of the voids to influence the failure mode by making propagation in one direction more favorable than in the other.

These double-notched specimens were also the first specimens to show spacing dependence on mode of failure. In the double-notched specimens, 80% of the random failures that occurred were in samples with the smallest spacing, which was 0.5 mm of solid material between consecutive voids. Most random failures were characterized by cracks nucleating near both edges of the specimen and propagating inward to meet near the center of the specimen. This significantly higher occurrence of random failure at smaller spacing suggests that as the spacing gets smaller, the anisotropy of the voids plays a less significant role, and the inter-void solid sections behave less like asymmetric solid regions and more like small fibers or ligaments. This idea is further supported by the numerical analyses reported in Table 0.1, which

shows a significantly smaller difference in toughness values between the favorable (forward) and unfavorable (backward) propagation modes when the spacing between voids is small. This spacing dependence also suggests that the many of the favorable failures seen at smaller spacings in the unidirectional specimens with only one edge notch may have been governed predominantly by the presence of the edge notch rather than by the asymmetry of the void arrangement itself.

0.6 Designing a "True Diode"

Analysis of the occurrence of favorable failure based on void orientation indicates that the asymmetry of the void structures plays a significant role in directional failure under unbiased loads. Despite this, even when the highest occurrence of favorable failure is considered, 78% for unidirectional diodes with only one notch, the favorable failure rate is still far too low to be considered behavior resembling that of a diode. However, using the knowledge gained from the analyses of these triangular void designs, heterogeneous structures can be made that have failure behavior resembling that of a diode.

The previous analyses demonstrated clearly that in order to obtain directional fracture behavior with high fidelity, both nucleation and propagation of the crack must be meaningfully controlled and constrained to minimize the number of possible failure occurrences that can arise from weakest link failure behavior. The importance of controlling nucleation is emphasized by the analysis of the mechanics of unfavorable failure. The analysis of unfavorable failure clearly demonstrates that even though void arrangement can make propagation of a crack preferentially less favorable in one direction, the location of the critical flaw in the system can still set the crack along a trajectory where a less favorable failure condition is the only reasonable means of releasing mechanical energy. Without any structural influence, nucleation of the crack from a critical flaw is dictated by weakest link theory, and because the printing process does not contain any spatial bias with respect to void arrangement, this nucleation should be random. However, if an asymmetric structure is to behave like a true fracture diode, this nucleation must be constrained such that the possible nucleation sites fall within regions where the asymmetric structure can effectively control propagation direction.

If true fracture diode behavior is to be achieved, once nucleation is properly controlled, propagation must have strong directional asymmetry. In the previous analyses with isosceles triangle voids, it was found that both void spacing and structure played

critical roles in the degree of toughness asymmetry seen during crack propagation. Fractographic analysis showed that in the case of unfavorable propagation, the crack would become pinned at a void and then nucleate at the triangle tip in the next consecutive void, and the energy required to achieve this was related to the distance between the pinning void and the tip of the next consecutive void. This spacing effect was also seen in the double-notched specimens, where once the spacing between voids became too small, the toughness asymmetry was not dramatic enough to discourage propagation in the unfavorable direction, and failure became effectively random.

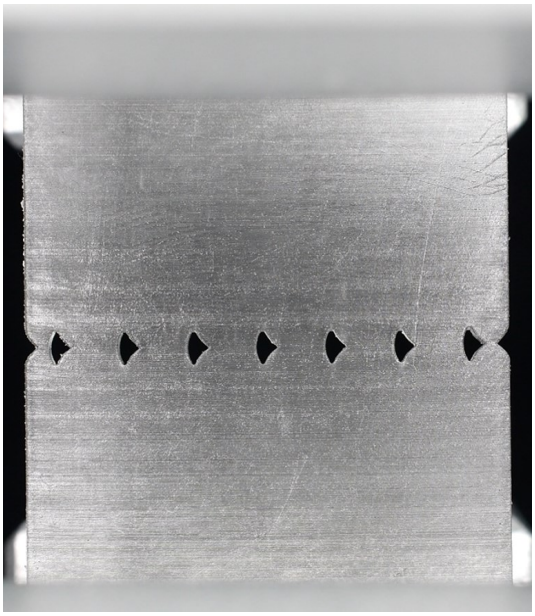

Figure 0.16: The "true diode" specimen design. In this design, the triangular voids were rounded and spaced further apart to increase toughness asymmetry and the solid segment size near the edges of the specimen were reduced to better control nucleation.

Using this information, a diode structure was designed that was able to effectively control both nucleation events as well as subsequent propagation. This design is shown in Figure 0.16. To better control nucleation without introducing bias, edge notches are introduced to both sides of the specimen to encourage nucleation from the edge of the specimen. Additionally, the solid segments near the edges of the specimen are much smaller in cross sectional area than the other inter-void spacings. This reduction in cross section near the free surface further encourages nucleation near the sides of the specimen by locally increasing the compliance in these regions. To better control propagation, this diode structure uses a rounded triangle void

design to further increase the toughness asymmetry between the favorable and unfavorable propagation modes. Additionally, void spacing is designed to make unfavorable propagation by nucleation at successive triangle tips even more difficult. This difficulty due to relatively large spacing is clearly evidenced in the numerical analysis of this diode structure shown in Figure 0.17. The larger spacing of the diodes significantly reduces the buildup of damage at the tips of successive triangles in backwards propagation, forcing much greater damage buildup at the rounded edge of the pinning diode, which requires significantly more energy to nucleate and propagate a crack. It is important to note, however, that this larger spacing effect does not scale monotonically. If the spacing of the voids becomes too far apart, the voids begin to act as isolated stress concentrators in an otherwise homogeneous matrix, and failure becomes governed the largest flaw within the homogeneous region between these voids. In this sense, choosing the spacing of the diodes is a balance between increasing spacing to discourage unfavorable propagation and reducing spacing to prevent weakest-link-governed failure. In the case of this investigation, the tailoring of this spacing was done empirically, but controlling the balance between these two effects is likely dependent on material processing, as this will dictate the resultant stiffness and toughness as well as the distribution of flaws within the material.

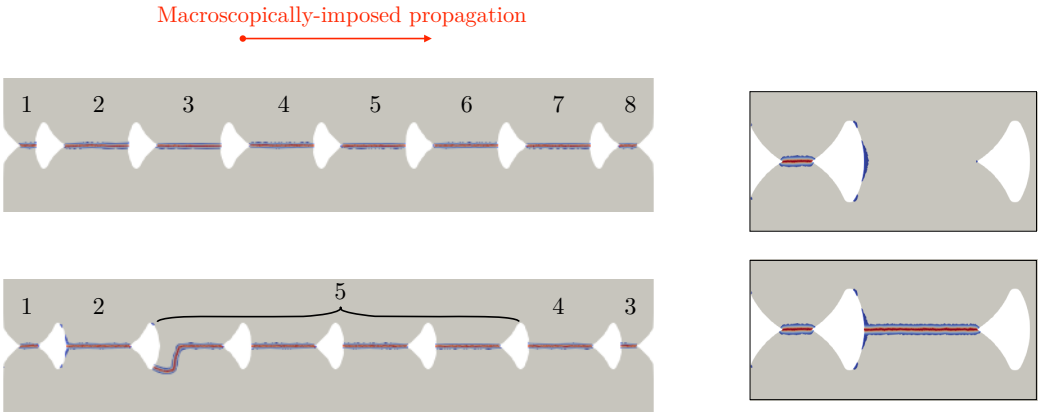

Figure 0.17: Numerical analysis of the true diode structure under surfing load conditions. (Left) Crack path in the forward and backward configuration, with numbers indicating the order of failed segments; (Right) Inset showing the fracture field in the backward specimen.

Using this true diode design, a total of 12 specimens were tested, and of these 100% failed favorably, indicating the potential for designed inclusions to produce controllable directional fracture. Even though fracture is a statistical phenomenon, sufficient control of both compliance and anisotropy can constrain the system enough

to produce a readily predictable outcome for both the nucleation and propagation of the crack. This controllable directional fracture could present significant opportunities for brittle materials in the context of a different approach to material optimization, where materials whose toughness cannot be sufficiently improved could be designed to instead fail in a way that minimizes catastrophic damage.

0.7 Summary

In this chapter, the influence of asymmetric void structure on failure behavior was explored using structures described as "fracture diodes". These structures used designs of triangular voids in different orientations to create directionally-dependent toughness behavior, which manifested as preferential directional failure under unbiased uniaxial tensile load. Several void designs were explored, including unidirectional and bidirectional arrangements as well as 3 different void spacings. Numerical simulations showed that the favorable failure direction was the direction of triangle convergence, and this was confirmed in experiment though both fractographic and statistical analysis. Analysis of the distribution of favorable failures for each arrangement showed that the presence of a notch at the edge of the specimen created some bias that encouraged failure from that edge, but introduction of symmetrical edge notches on both sides of the specimen reduced this bias. Finally, a "true diode" design was developed that used rounded triangles and carefully controlled void spacing to further enhance toughness asymmetry, resulting in favorable directional failure 100% of the time.

REFERENCES

[1] M. Z. Hossain, C. J. Hsueh, B. Bourdin, and K. Bhattacharya. Effective toughness of heterogeneous media. *Journal of the Mechanics and Physics of Solids*, 71(1):15–32, 2014. ISSN 00225096. doi: 10.1016/j.jmps.2014.06.002. URL http://dx.doi.org/10.1016/j.jmps.2014.06.002.

[2] B. Bourdin, G.A. Francfort, and J-J. Marigo. Numerical experiments in revisited brittle fracture. *Journal of the Mechanics and Physics of Solids*, 48(4):797–826, apr 2000. ISSN 0022-5096. doi: 10.1016/S0022-5096(99)00028-9. URL https://www.sciencedirect.com/science/article/pii/S0022509699000289.

[3] Blaise Bourdin, Gilles A. Francfort, and Jean-Jacques Marigo. The Variational Approach to Fracture. *Journal of Elasticity*, 91(1-3):5–148, apr 2008. ISSN 0374-3535. doi: 10.1007/s10659-007-9107-3. URL http://link.springer.com/10.1007/s10659-007-9107-3.

[4] Satish Balay, William D. Gropp, Lois Curfman McInnes, and Barry F. Smith. Efficient Management of Parallelism in Object-Oriented Numerical Software Libraries. In *Modern Software Tools for Scientific Computing*, pages 163–202. Birkhäuser Boston, Boston, MA, 1997. doi: 10.1007/978-1-4612-1986-6_8. URL http://link.springer.com/10.1007/978-1-4612-1986-6{_}8.

[5] S. Balay, S. Abhyankar, M. Adams, J. Brown, P. Brune, K. Buschelman, L. D. Dalcin, V. Eijkhout, W. Gropp, D. Kaushik, M. Knepley, D. May, L. Curfman McInnes, T. Munson, K. Rupp, P. Sanan, B. Smith, S. Zampini, H. Zhang, and H. Zhang. PETSc Users Manual Revision 3.8. Technical report, Argonne National Laboratory (ANL), Argonne, IL (United States), sep 2013. URL http://www.osti.gov/servlets/purl/1409218/.

[6] S. Balay, J. Brown, K. Buschelman, W.D. Gropp, D. Kaushik, M. Knepley, L.C. McInnes, B. Smith, and H. Zhang. PETSc/Tao: Home Page, 2013. URL https://www.mcs.anl.gov/petsc/.

[7] G.P. Cherepanov. Crack propagation in continuous media: PMM vol. 31, no. 3, 1967, pp. 476–488. *Journal of Applied Mathematics and Mechanics*, 31(3):503–512, jan 1967. ISSN 0021-8928. doi: 10.1016/0021-8928(67)90034-2. URL https://www.sciencedirect.com/science/article/pii/0021892867900342.

[8] A. A. Griffith. The Phenomena of Rupture and Flow in Solids. *Philosophical Transactions of the Royal Society A: Mathematical, Physical and Engineering Sciences*, 221(582-593):163–198, jan 1921. ISSN 1364-503X. doi: 10.1098/

rsta.1921.0006. URL http://rsta.royalsocietypublishing.org/cgi/doi/10.1098/rsta.1921.0006.

[9] James R Rice. Mathematical Analysis in the Mechanics of Fracture. Technical report, 1968. URL http://esag.harvard.edu/rice/018{_}Rice{_}MathAnalMechFract{_}68.pdf.

[10] C-J. Hsueh, L. Avellar, B. Bourdin, G. Ravichandran, and K. Bhattacharya. Stress fluctuation, crack renucleation and toughening in layered materials. *Journal of the Mechanics and Physics of Solids*, 120:68–78, nov 2018. ISSN 0022-5096. doi: 10.1016/J.JMPS.2018.04.011. URL https://www.sciencedirect.com/science/article/pii/S0022509617311407.

[11] M Y He and J W Hutchinson. Crack Deflection at an Interface Between Dissimilar Elastic-Materials. *Int J Solids Struct*, 25(9):1053–1067, 1989.